CrystEngComm

Accepted Manuscript

This is an *Accepted Manuscript*, which has been through the Royal Society of Chemistry peer review process and has been accepted for publication.

Accepted Manuscripts are published online shortly after acceptance, before technical editing, formatting and proof reading. Using this free service, authors can make their results available to the community, in citable form, before we publish the edited article. We will replace this *Accepted Manuscript* with the edited and formatted *Advance Article* as soon as it is available.

You can find more information about *Accepted Manuscripts* in the Information for Authors.

Please note that technical editing may introduce minor changes to the text and/or graphics, which may alter content. The journal's standard Terms & Conditions and the Ethical guidelines still apply. In no event shall the Royal Society of Chemistry be held responsible for any errors or omissions in this *Accepted Manuscript* or any consequences arising from the use of any information it contains.

ROYAL SOCIETY OF CHEMISTRY

www.rsc.org/crystengcomm

Structural and optical characterizations of ball milled copper doped bismuth vanadium oxide ($BiVO_4$)

Victor-Ishrayelu Merupo[a,b], Subramaniam Velumani [a], Karolina Ordon[b,c], Nicolas Errien[b], Jacek Szade[d] and Abdel-Hadi Kassiba[b**]**

Received (in XXX, XXX) XthXXXXXXXXX 20XX, Accepted Xth XXXXXXXXX 20XX

DOI: 10.1039/b000000x

Copper doped $BiVO_4$ nanoparticles were synthesized by mechano-chemical method under optimized conditions to obtain monoclinic scheelite structure. Crystal structure and its evolution with doping were investigated by X-ray powder diffraction, micro-Raman spectroscopy, field effect-scanning electron microscopy (FE-SEM) and high resolution transmission electron microscopy (HRTEM). Spherical shape particles with size ranging between 40-160 nm were obtained possessing monoclinic scheelite structure. From the structural data analysis it can be observed that the particle size decreases and distortions occur as the copper content increases in doped $BiVO_4$. Chemical bonding and valence states of the Bi-4f, V-2p, O-1s and Cu-2p ions were investigated by XPS which revealed the location of Cu ions in the host lattice of $BiVO_4$ in agreement with EPR investigations. UV-Visible absorption experiments showed broad band in the visible range with small shift of the energy band-gap from 2.41 eV for undoped $BiVO_4$ to 2.34 eV for 10 at.% Cu-$BiVO_4$. Additional absorption band shoulders and widening of the optical absorption spectrum in the visible range with well crystalline monoclinic scheelite structure paves the way for efficient visible light driven photocatalytic activity.

Due to environmental requirements for preservation of water and earth atmosphere, new photocatalytic materials have become subject of intensive research during the last decade.[1] Particularly, devices using functional semiconducting oxides is the matter of interest in the search for an alternative renewable, clean and sustainable energy.[2] The environmental or energy applications of such materials are purely based on photocatalytic reactions catalyzed by the solar spectrum. The efficiency of these photocatalysts depends on their ability to absorb a large fraction of solar spectrum including the visible part. Several classes of materials were then developed for various applications. They are exploited in hydrogen production by water dissociation or for environmental protection for water and atmosphere depollution by degradation of pollutants generated by industrial or human activities. In this context, the most popular photocatalyst used so far is titanium dioxide (TiO_2) which was subject of impressive number of reports during the last two decades. Though it possesses a large band gap (3.2 eV), TiO_2 as a photocatalyst has shown a high efficiency only in the UV spectral range; i.e. 4-6% of the solar irradiation spectrum.[3]

The search for alternative functional semiconducting oxides was motivated by the need to develop visible light active systems based on bismuth vanadate ($BiVO_4$) as reported recently by our group[4] and also its well-known ferroelasticity and ionic conductivity.[5] It has been previously shown that $BiVO_4$ is a potential candidate in several solar radiation driven applications including water splitting for hydrogen production and degradation of organic pollutants.[6] These performances are also associated with low cost and high stability in aqueous media as a visible light driven photocatalyst.[7] However, the photocatalytic reactions are highly dependent on the structural polytypes of the material which influences the electronic and optical behaviours. $BiVO_4$ crystallizes in three different forms viz., monoclinic scheelite, tetragonal scheelite and tetragonal zircon. According to previous reports, photocatalytic activity of the monoclinic phase $BiVO_4$ shows better efficiency compared to tetragonal zircon and tetragonal scheelite structure.[8] From theoretical and numerical calculations based on DFT, it is found that the effective hybridization of Bi 6s state and O 2p state as upper valence band (HOMO) with V 3d states as lower conduction band (LUMO) would be responsible for the low bandgap of 2.4 eV in the $BiVO_4$ monoclinic scheelite structure.[9]

Despite stabilizing monoclinic scheelite phase with different morphologies as nanosized objects (nanoparticles, nanorods, nanowires etc.), pure $BiVO_4$ shows relatively low photocatalytic efficiency under visible light.[10] The problem of electron-hole pair photogeneration in the visible range with short life-times and high rates of charge carrier recombination requires improvement by relevant approaches to overcome such limitations. Recently Yao *et al.* reported that the mesoporous structure of $BiVO_4$ represents good option to overcome these shortcoming.[11] However, the strategy of doping $BiVO_4$ structure by suitable metallic elements such as transition metal ions is expected to optimize the electronic features required for photocatalysis. Thus, substitutional doping of $BiVO_4$ with defined rates up to 10 at.% with a stable monoclinic structure is a challenging task with the aim to fine-tune the optical and chemical properties.[12] Previously, Xu *et al.* synthesized Fe, Co and Cu- loaded $BiVO_4$ by wet impregnation method and found that the Cu-loaded $BiVO_4$ has shown highest photocatalytic activity amongst all other transition metals.[13] So far, doped $BiVO_4$ were synthesized by several methods such as Sol-gel,[11] hydrothermal,[13] impregnation method,[14] solution combustion,[15] solid-state reaction,[16] co-precipitation [17] and metal organic decomposition.[18] Venkatesan *et al.* reported that high energy ball milling technique is one of the simple and effective pathway to achieve highly monoclinic $BiVO_4$ particles with average crystalline domain size of 20 nm and an energy band gap (E_g = 2.36 eV).[4]

The present work is dedicated to ball milled $BiVO_4$ with Cu-doping. The optimized synthesis parameters such as ball per powder (BPR) ratio and rotation speed of synthesis chamber per min (rpm) were defined from our previous reports.[4] Post-

CrystEngComm Accepted Manuscript

synthesis treatments were performed to improve the structural features such as pure crystalline phase and substitution of Cu ions inside the crystal sites of $BiVO_4$. To achieve such tasks, characterization techniques including micro Raman and X-ray powder diffraction (XRD) for structural studies, Field emission Scanning electron microscopy (FE-SEM) and High resolution transmission microscopy (HR-TEM) for the morphology, particle size and homogeneity of the chemical materials, were used. These studies were also supported by X-ray photoelectron spectroscopy (XPS) which probes the involved chemical bonding. As Cu^{2+} are paramagnetic ions, electron paramagnetic spectroscopy (EPR) was performed on several doped samples to evaluate the degree of substitution and to inform about the distribution of doped copper inside the synthesized materials. The evolution of the optical band gap was investigated and correlated with the structural and electronic changes induced by Cu doping.

Experimental details

Synthesis

The high energy ball milling (HEM) technique is a suitable process for producing large scale, micro- and nanosized materials for several applications. HEM synthesis is based on a strong mechanical energy transfer created by colliding hard phase materials like carbides or ceramics with reactants such as metals, alloys, optimized composites. During the HEM process, repeated fracturing and welding ensures that the milling operations will lead to the solid state reaction of the individual materials resulting in the formation of the final composite materials. By this means, doping or alloying chemical elements can form micro- or nanostructured powders with defined stoichiometry and crystalline order. Fig.1 illustrates the main steps involved in HEM synthesis.

For the synthesis of Cu doped $BiVO_4$ powders, the starting materials are bismuth oxide (Bi_2O_3, Sigma Aldrich 99.99%), vanadium oxide (V_2O_5, Sigma Aldrich 99.97%) and metallic copper grains (Sigma Aldrich <1mm, 99.9%). The reactants were used at different atomic percentages (x = 1, 5 and 10 %) in a stoichiometric ratio of ***[1 : (1-x) : x]*** and blended homogenously by using agate mortar for the total mixture weight of 7.7 grams which is equal to the weight of one tungsten carbide (WC) ball and loaded inside 80 ml WC made jar with balls of 9 mm diameter. Retsch-planetary high energy ball mill PM 400 was used and the milling was performed for 6 hours at 400 rpm with 10:1 BPR ratio. The as-prepared doped Cu-$BiVO_4$ samples were annealed at 450^{o}C for 2 hours under air atmosphere to improve the crystallinity. In the forthcoming sections, the prepared samples were referred to as A, B, C and D for undoped $BiVO_4$, 1 at.%, 5 at.% and 10 at.% of copper in Cu-$BiVO_4$ respectively.

Characterization techniques

XRD patterns were recorded by using a PANalytical-powder diffractometer with Cu Kα radiation (λ=0.15418 nm) under accelerating voltage of 30 KV and emission current of 20 mA. The used scale of 2θ angle was ranging from 18 to 52°. The optical properties were investigated by UV-Vis diffused reflectance method by using Varian Cary 500 UV-Vis- NIR spectrometer in a wavelength range from 350 nm to 800 nm. Raman spectra were obtained with a Horiba Jobin Yvon Lab Ram-HR 800 Raman micro-spectrometer using an excitation line of He-Ne –laser at 632.18 nm. The surface morphology and chemical compositions were characterized by FE-SEM, Carl Zeiss Auriga 60 (high vacuum, spot size 7.5 µm, 10 kV accelerating voltage) coupled with an Energy-dispersive x-ray spectroscope (Bruker, PB-ZAF method, Sensor 5010, 129 eV resolution). HR-TEM observations were carried out on JEOL ARM200F instrument operated at 200 kV accelerating voltage. EPR spectra were recorded in X-band (9.4 GHz) at 150 K temperature by using Bruker EMX spectrometer with cryogenic cryostat from Oxford Instruments. The resonance positions of EPR lines were accurately evaluated by using a characteristic EPR line of dry DPPH sample associated to g-factor of 2.0036. XPS was used to determine binding energies (BEs) related to molecular bonds of Bi, V, O and Cu involved at the surface of Cu-$BiVO_4$ particles. Spectra were recorded by XPS, PHI 5700 system with an Omni Focus IV lens system (Physical Electronics Inc.) with monochromatic Al Kα X-ray source with the C1s signal at 284.6 eV used as a reference for BEs calibration.

Results and discussion

Structural features from XRD studies

Diffraction patterns of Cu–$BiVO_4$ nanoparticles at different Cu concentrations exhibit monoclinic scheelite phase according to the standard JCPDS data (014-0688) depicted in Fig.2 along with Cu-$BiVO_4$ refined pattern. It has been noticed that the high intense diffraction peak (-121) corresponding to the Cu-$BiVO_4$ samples shifts towards a higher angle (2θ) compared to pure $BiVO_4$ as shown in inset of Fig. 2. This shift occurs from structural distortions such as compressive strains due to the incorporation of copper into the crystal sites of $BiVO_4$ structure. The diffraction angle lines N {denoted by $N= h^2 + k^2 + l^2$} such as 2 (110, 011), 4 (200, 002), 6 (211, -112), 14 (231, 132), 20 (240, 042) doublet peaks were merging for highly doped Cu-$BiVO_4$ samples. The intensity of the lines depend on the arrangement of atoms in the unit cell. The decrease in the intensity and an increase in the FWHM of the diffraction lines can be induced by a disorder in the location of Cu inside the lattice or by distortions due to size differences between substituted ions. It is worth noting that all the as-prepared samples were annealed at the same temperature i.e. 450°C, which is defined from the best improvement of the crystal structure for undoped sample. However, this temperature cannot be optimized to reproduce the good crystalline structure in heavily Cu doped $BiVO_4$.

Crystal domain sizes of $BiVO_4$ and Cu-$BiVO_4$ were calculated from Scherrer's formula and reported in Table1. The calculations consider the XRD line broadening FWHM values subtracted from the standard FWHM of the used reference LaB_6 fixed at Δ(2θ)=0.046°. The average size of crystalline domains in Cu-$BiVO_4$ is situated in the range 33– 40 nm with the lowest size in the heavily doped sample. The disorder of the copper ions distribution in the lattice and the shift of the annealing

CrystEngComm Accepted Manuscript

temperature required for improved crystalline structure are plausibly the reason of increased FWHM diffraction lines with the doping rates.

The doping process alters the crystallographic lattice parameters as illustrated below for 10 at.% doped sample. Indeed, crystal unit cell dimensions were refined by Rietveld method using MAUD software. The diffraction patterns for doped and undoped samples were adjusted to standard monoclinic system with space group I2/c. The refined datas such as lattice parameters and characteristic 2θ shifts are summarized in table 2a and depicted in Fig. 3 for various Cu doping rates. The refined crystallographic data reveals a reduction of lattice parameters with the amount of Cu-doping. The atomic positions of Bi, V, O1 and O2 summarized in table 2b indicate lattice compression in the direction of crystallographic axes a and c and suggests also a compression in V-O covalent bonds of the VO_4 tetrahedron.[9] However, no drastic change seems to alter the weak molecular bonds of Bi-O, involved in dodecahedron arrangements. Since the calculated atomic radius of Cu (1.45 Å) is less than V (1.71 Å), the incorporation of Cu ions in $BiVO_4$ matrix as substitution to V ions leads to a reduction of the lattice parameters.[20] Structural distortions in VO_4 tetrahedron are expected to induce an internal electric field that contributes to the separation of electron-hole pairs. This is of particular interest for the photocatalytic processes as expected from metal doped $BiVO_4$ materials.[9]

Raman investigations of vibrational features

Raman scattering spectroscopy is an efficient tool for probing the structure and bonding in metal–oxide species through their vibrational characteristics. In the monoclinic phase of $BiVO_4$, the Raman spectra (Fig. 4) exhibits six noticeable vibrational bands at 210, 327, 367, 637, 702 and 826 cm^{-1} which are related to the vibrational features of VO_4 tetrahedron.[21] The intense band at 826 cm^{-1} was attributed to the shorter symmetric V–O stretching mode (A_g) and the weak bands at 702 and 637 cm^{-1} were assigned to the long (Ag) and short (Bg) asymmetric V–O stretching modes respectively. The asymmetric and symmetric bending vibrations of the VO_4 tetrahedron were detected at 327 and 367 cm^{-1}, respectively according to the assignment reported elsewhere.[22]

By using higher doping rates as 5 at.% and 10 at.%, the V–O stretching modes (819, 821 cm^{-1}) of the Cu-$BiVO_4$ are shifted to a lower wavenumber as compared to the pure sample or for low doping rate (i.e. 1 at. %). Such results are consistent with elongation of bond length of V–O for highly Cu doped $BiVO_4$ samples. Similar effects were reported in $BiVO_4$ grown by wet chemistry under different conditions where the shift of Raman bands is attributed to structural distortions which are induced by modified electronic band structures of $BiVO_4$.[23] In addition to the behaviour of the Raman band intensities, the FWHM of the major Raman band associated to symmetric stretching mode at 826 cm^{-1} expands with Cu content as illustrated in Fig. 8. This behaviour correlates with the degree of crystallinity or defects including oxygen vacancies. Similar effects were reported previously with other doping element as cobalt leading to shifts and overlap of the Raman bands of VO_4 tetrahedrons.[24] The analysis of the Raman spectra corroborates the conclusions inferred from XRD investigations and gives consistent support to the structural evolution induced by Cu-doping in monoclinic scheelite phase of $BiVO_4$.

Particle morphology and structure probed by FE-SEM and HR-TEM

FE-SEM microscopy images of Cu-$BiVO_4$ nanoparticles show a spherical shape and sizes ranging from 40-160 nm (Fig. 5). The particles are found to be composed by small and nanosized grains. The "image J 1.48v" software was used for the quantitative evaluation of the particle size distribution. Noticeable reduction in the particles sizes was clearly seen for higher Cu doped samples as traduced by particle size distribution plots reported in the inset. The main reason lies in the effect of Cu incorporation on the thermodynamic properties of the ball milled powders as previously attributed to the fact that Cu-doping of $BiVO_4$ inhibits the particle growth.[25] The elemental composition analysis was performed by EDAX for Cu-$BiVO_4$ nanoparticles and their atomic (at.) % values are summarized in table 3. Chemical element distribution mappings were also carried out for Bi, O, V and doping ions Cu as illustrated in the same Fig. 5. Within the uncertainty of the EDAX, homogenous distributions of elements were inferred, testifying the absence of agglomeration or some phase segregations.

HR-TEM analysis of Cu-$BiVO_4$ particles reveals well crystalline domains (Fig 4B inset) through the resolved crystal lattice fringes for the considered samples (A, B, C, and D) with corresponding FFT crystallographic planes (Fig. 6). The inter-reticular distances d_{hkl}, in the crystalline monoclinic phase, were calculated for all the samples and the obtained values are associated to d_{110} = 0.474 nm, d_{011} = 0.467 nm, d_{040} = 0.312 nm and d_{220} = 0.237 nm. Although distortions of the lattice parameters were demonstrated with increased rates of Cu-doping, HR-TEM observations show good crystalline quality of doped samples.

Chemical bonding inferred from XPS investigations

As far as the chemical bonding with Cu ions is concerned, XPS analysis is a method of choice to probe the molecular bonding. XPS patterns were recorded on representative samples of Cu–$BiVO_4$. As shown in Fig. 7a, XPS spectra reveal the binding energy levels of Bi 4f, V 2p, O 1s and Cu 2p. The binding energies of Cu species taking into account the spin orbital splitting of 2p core level were found at E_b =933 eV and 953 eV associated to the spectroscopic terms Cu-$2p_{1/2}$ and Cu-$2p_{3/2}$ doublet peaks respectively as illustrated in Fig. 7b. As can be seen from the XPS curves, the Cu-$BiVO_4$ sample possesses binding energies suggesting the presence of copper in oxidized form such as CuO or Cu_2O. In Fig. 7c, the XPS spectra related to Bi – 4f, consist in two intense and symmetrical peaks at E_b = 159.8 and 165.1 eV, corresponding to the Bi - $4f_{7/2}$ and Bi - $4f_{5/2}$ terms, respectively in accordance with Bi ions in their trivalent

CrystEngComm Accepted Manuscript

oxidation state. The XPS spectrum of V $2p_{3/2}$ depicted in Fig. 7d can be de-convoluted into two peaks with energies E_b = 515.5 and 516.4 eV attributed to the surface V^{4+} and V^{5+} species respectively. As a matter of fact, the stable oxidation state V^{5+} can be converted to V^{4+} due to surface effect (nanoparticles) or when oxygen vacancies are involved.[4]

For oxygen, O1s XPS spectra in Cu-$BiVO_4$ samples are shown in Fig. 7(e). The asymmetric peak centred at 530 eV was deconvoluted into two components. Different bonding states of the oxygen content coexist and associated to the binding energies E_b = 529.4 and 531.2 eV. Such values are assigned to lattice oxygen (O_{latt}) and adsorbed oxygen (O_{ads}) species respectively.[26] However, the O_{ads}/O_{latt} molar ratios are relatively high for all the samples irrespective to the powders morphologies and the doping rates. XPS results which are more sensitive to surface compositions, are completed as discussed below, by EPR experiments which probes precisely the Cu^{2+} and V^{4+} ions for their absolute concentrations as well as their local environments in the samples.

EPR studies of Cu-doped $BiVO_4$

EPR spectroscopy is a sensitive tool to probe the doping process or surface effects where the oxidation state of particular ion leads to electronic configurations with unpaired spins. The situation of monoclinic $BiVO_4$ structure doped by copper ions is worthy of interest. Indeed, in perfect crystalline structure, vanadium ions possess the valence state V^{5+} state leading to spinless ions. However, due to oxygen vacancies induced notably in nanosized particles with high specific surfaces, the departure of vanadium to its normal valence state leads to reduced species as V^{4+} which are paramagnetic ions. The electronic configuration of V^{4+} ($3d^1$) possesses an effective electronic spin (S=1/2) giving rise to an EPR signal. For copper doping of $BiVO_4$, oxygen environment stabilizes the oxidation state Cu^{2+} with an electronic configuration ($3d^9$) giving rise to an EPR signal with an electronic spin S=1/2. The EPR spectra of Cu-$BiVO_4$, are summarized in Fig.8a for different doping ratios. Each EPR spectrum is composed of two contributions traduced by a central isotropic sharp EPR line superimposed to broad and structured resonance band. The experimental EPR spectra were adjusted by using Bruker-Winsinfonia software. Thus, the single EPR line is associated to V^{4+} ($3d^1$) with regard to the magnetic interaction marked by an isotropic g-Landé tensor with diagonal components $g_x = g_y = g_z = 1.97$. The EPR signal associated to Cu^{2+} ions is accounted by an anisotropic magnetic Landé tensor $g_x = 2.15$, $g_y = 2.07$ and $g_z = 2.35$.The Cu^{2+} EPR line width (100-200 Gauss) and also V^{4+} (100 Gauss) as well as the unresolved hyperfine structures for both ions are accounted by dipolar or exchange interactions between copper and vanadium ions situated at relatively short distances. In other words, this effect traduces the possibility of agglomerated paramagnetic species. On the other hand, the rate V^{4+}/V^{5+} is more important for low copper doping rates and drastically decreases with increased copper concentrations in the samples. Meanwhile, the evolution of the EPR spectrum intensity related to copper ions didn't follow the initial doping rate. Such behaviour is plausibly due to the occurrence of efficient charge transfer between Cu^{2+} and V^{4+} as well as the suppression of oxygen vacancies which contributes to the creation of reduced vanadium. Quantitatively, the absolute concentrations of these ions were obtained from the double integration of the EPR spectra related to each paramagnetic ion and using a reference sample (CuSO4) with calibrated spin concentration. The results summarized in fig.8b give a quantitative evaluation of Cu^{2+} content in the investigated samples as well as active electronic centres as V^{4+}. Concentrations of Cu^{2+} were found to increase with the doping rate from 0.8 $X10^{17}$ (initial doping 1at.%) up to 2 $X10^{17}$ ion/gram (initial 10 at.%). For vanadium ions V^{4+}, a decrease of its concentration from 1.2 $X10^{17}$ down to 0.3 $X10^{16}$ spin/gram occurs with increasing the doping from 1 at% to 10 at.%.

To sum up, the EPR experiments show the existence of reduced valence states of vanadium ions (V^{4+}) along with oxidized environments of copper ions (Cu^{2+}). The effective concentration of Cu^{2+} in the samples is evaluated with good accuracy. Dipolar or exchange interactions are involved between copper and vanadium ions as well as charge transfer between these species. This process contribute to the photocatalytic activity of Cu-$BiVO_4$ materials as shown in the supplementary data associated to this article (Fig.S1).

UV-Visible optical absorption of $BiVO_4$ powders

The optical absorption spectrum of a semiconducting material is monitored by its electronic structure which defines the threshold and the concerned spectral range. The doping process is dedicated to extend the optical absorption on a larger visible range leading to visible light driven photocatalysis. In the case of undoped $BiVO_4$, the main absorption band is expanded on the wavelength range 350-530 nm. In doped Cu-$BiVO_4$ powders, broad shoulder and extended absorption background appear on the main band over the range of 530 - 800 nm and their importance correlate with the Cu content as depicted in Fig. 9A. By using the Tauc plot based on the absorbance and incident photon energy hν, the following relation (equation 1) serves to evaluate the direct band gap value:

$$\alpha.h\nu = A(h\nu - E_g)^{n/2} \quad (1)$$

α, A, n and Eg represent the absorption coefficient, a constant of proportionality, index with different values (1, 3, 4, 6) depending on the nature of optical transition and the direct band gap energy respectively. The threshold absorption edges were evaluated by an asymptotic extrapolation (Fig. 9B) for the pure sample and for Cu-doped $BiVO_4$ with the doping rates about 1, 5 and 10 at.%. The obtained values were respectively 2.41, 2.40, 2.37 and 2.34 eV for the "pseudo-direct" band gap of $BiVO_4$. The term "pseudo" is used due to a favourable direct transition between (VB) and (CB) which occurs outside the Brillouin zone center.[27] Indeed, the minimum of conduction band (CBM) is located at the Z point which corresponds to (0.000, -0.500, 0.500) direction in the Brillouin zone.[28] In addition to fundamental absorption

CrystEngComm Accepted Manuscript

threshold edges, broad shoulders are observed at 2.01 and 1.98 eV in the 5 and 10 at.% Cu doped samples respectively. The involved atomic orbitals in (VB) are constituted by Bi (6s) and O (2p) while they are composed by V (3d) states for (CB). The optical band gap is then defined by transitions between (VB) and (CB) with finite probability at the Z point. In the doped samples, copper ions contribute in one hand to lower the band gap by introducing allowed states within the band gap. On the other hand, the Cu-O environments demonstrated by EPR and XPS favours the occurrence of transitions between O (2p) and Cu (3d). The broad shoulder on the main absorption band can be accounted by the copper doping in agreement with large effect with increasing the doping rate. This effect correlates well with the colour of Cu doped $BiVO_4$ samples being changing from bright yellow (pure $BiVO_4$) to dark brown as shown in Fig. 9A inset. The colour change is a feature of a semiconductor material, which is dependent on its electronic structure and considered as an important factor for photocatalytic activity.[29] The broad background absorption can be accounted by intermediate electronic levels induced in the band gap by Cu substitution in the host crystal sites. This effect enhances the photocatalytic efficiency compared to undoped materials as reported in the supplementary data (Fig.S1).

Conclusion

Cu doped $BiVO_4$ nanoparticles were synthesized by mechano-chemical technique with improved processing parameters and post-synthesis treatments to optimize the crystal structure. Thus, monoclinic scheelite structure was obtained for representative samples with different Cu doping ratios. XRD and micro-Raman investigations were analyzed by considering structural distortions with quantitative estimation of the lattice parameters and the lattice compression as function of the Cu doping rates. Spherical nanoparticles distributed in the range 40 - 160 nm were estimated from FE-SEM images with the tendency to decrease their sizes for higher Cu doped samples. XPS analysis determined the chemical bonding involved between the constitutive elements and including the Cu location in the host lattice. Mixed oxidation states of V^{4+}/V^{5+} with variable concentrations were shown from XPS spectra also supported by EPR experiments and correlate with the Cu doping ratios. The effective concentrations of copper ions in the valance state Cu^{2+} as well as that of the reduced form of vanadium ions V^{4+} were quantitatively determined by EPR. The features of the EPR spectra and the evolution of these concentrations with the copper doping rate indicates the occurrence of interactions and charge transfer between these electronic active species. These results suggest that the mechanism of charge transfer required for photocatalysis reactions would be affected by Cu doping. Finally, UV-Vis optical absorption bands show an extension in the spectral range 530-800 nm by Cu doping. This evolution of optical features is of particular interest for visible light driven photocatalysis based on stabilized scheelite monoclinic structure in Cu-$BiVO_4$

Acknowledgment

V. I. Merupo gratefully thanks the financial supports given by CONACYT – Becas mixtas, Mexico and Doctoral School 3MPL – University of Maine, Le Mans, France. K. Ordon has benefited from financial support of Polonium program 31 300 TA provided by French Embassy in Warsaw. The authors would like to thank Prof. Alain Bulou for Micro-Raman spectrometry measurements and Alvaro Angeles for HR-TEM characterizations from LANE Cinvestav-IPN. We thank the financial support extended from the project between Cinvestav-University du Maine joint funds.

Notes

[a] *Department of Electrical Engineering (SEES), CINVESTAV-IPN, Zacatenco, Av IPN #2508, Col Zacatenco, D.F., C.P. 07360, Mexico. Fax: +52 5557474003; Tel: +52 5557474001;Email: velu@cinvestav.mx*
[b] *Institute of Molecules & Materials of Le Mans (IMMM) UMR CNRS, Universite du Maine, 72085 Le Mans, France. Fax: +33 (0)243833518; Tel.: +33 (0)243833512; Email: kassiba@univ-lemans.fr*
[c] *Institute of Physics, Jan Dlugosz University in Czestochowa, 13/15 Al.Armii Krajowej, 42 200 Czestochowa, Poland.*
[d] *A.Chełkowski Institute of Physics and Silesian Centre of Education and Interdisciplinary Research - University of Silesia, Ul. Uniwersytecka 4, 40-007 Katowice, Poland.*
[**] *Corresponding authors*

References

1 (a) M. H. Alonso, F. Fresno, S. Suarez and J.M. Coronado, *Energy Environ. Sci*., 2009,**2,** 1231-1257; (b) M.R. Hoffmann, S. T. Martin, W. Choi, and D. W. Bahnemannt, *Chem. Rev.*,1995, **95(1),** 69-96; (c) Q. Xiang, Jiaguo Yu and M. Jaroniec, *Chem. Soc. Rev.*, 2012, **41,** 782-796; (d) A.O. Ibhadon and P. Fitzpatrick, *Catalysts*, 2013, **3(1)**, 189-218; (e) H. Xu, S. Ouyang, L. Liu, P. Reunchan, N. Umezawaace and J. Ye, *J. Mater. Chem. A*, 2014, **2**, 12642-12661.
2 (a) X. Chen and S.S. Mao, *Chem. Rev*., 2007, **107,** 2891-2959; (b) W. Doerffler and K. Hauffe, *J. Catalysis.*, 1964, **3**, 171-178; (c) F. Steinbach, *Nature*, 1969, **221**, 657-658; (d) T.K. Townsend, N. D. Browning and F.E. Osterloh, *ACS Nano*, 2012, **6(8)**, 7420-7426; (e) A A. Ashkarran, A.I. Zad, M.M Ahadian and S A.M Ardakani, *Nanotechnology*, 2008, **19**, 195709 (7pp).
3 D. L. Liao and B.Q. Liao, *J photochem photobiol A*, 2007,**187**, 363.
4 (a) R. Venkatesan, S. Velumani and A. Kassiba, *Mat. Chem. Phys.*, 2012, **135 (2, 3)**, 842-848; (b) R.Venkatesan, S.Velumani, M.Tabellout, N. Errien and A. Kassiba, *J. Phys. Chem. Sol.*, 2013, **74 (12),** 1695-1702.
5 (a) Y. T. Ho, C. S. Ho, S.K. Jeong and J. M. Su, *J. Phys Condens. Matter*, 1994, **6**, 383-392; (b) I.C. Vinke, J. Diepgrond, B.A. Boukamp, K.J. de Vries and A.J. Burggraaf, *Solid State Ionics*, 1992, **57**, 83-89.
6 (a) J. Su, L. Guo, N.Bao and C. A. Grimes, *Nano Lett.*,2011, **11**, 1928-1933; (b) H. Jiang, H. Endo, H. Natori, M. Nagai and K. Kobayashi, *Mater. Res. Bull*, 2009, **44**, 700-706.
7 A. Walsh, Y. Yan, M.N. Huda, M. M. Al-Jassim, and Su Wei, *Chem. Mater.*, 2009, **21**, 547-551.
8 (a) S. Tokunaga, H. Kato and A. Kudo, *Chem. Mater.*,2001, **13(12)**, 4624-4628; (b) X. Zhang , Z. Ai , F.Jia, L. Zhang, X.Fan and Z. Zou, *Mat. Chem. Phys.*,2007, **103**, 162-167.
9 (a) Z. Zhao, Z. Li and Z. Zou, *Phys. Chem. Chem. Phys.*, 2011, **13**, 4746-4753; (b) H.S. Park, K.E. Kweon, H. Ye, E. Paek, G. S. Hwang and A.J. Bard, *J. Phys. Chem. C*, 2011, **115**, 17870-17879.
10 (a) H. Fan, D. Wang, L. Wang, H. Li, P. Wang, T. Jiang and T. Xie, *Appl. Surf. Sci.*, 2011, **257**, 7758-7762; (b) H. Li, G. Liu, S. Chen, Q. Liu and W. Lu, *Physica E*,2011, **43**, 1323; (c) J. Su, L. Guo, S. Yoriya and C. A. Grimes, *Cryst. Growth & Des.*, 2010, **10(2),** 856-861.

CrystEngComm Accepted Manuscript

11 M. Yao, M. Liu, L. Gan, F. Zhao, X. Fan, D. Zhu, Z. Xu, Z. Hao and L. Chen, *Colloids Surf., A*, 2013, **433**, 132-138.

12 M. Wang, H. Zheng, Q. Liu, C. Niu, Y. Che and M. Dang, *Spectrochim. Acta A*, 2013, **114**, 74-84.

13 H. Xu, H. Li, C. Wu, J. Chu, Y. Yan and H. Shu, *Mater. Sci. Eng. B*, 2008, **147**, 52-56.

14 H. Jiang, H. Dai, X. Meng, L. Zhang, J. Deng, Y. Liu and C. T. Au, *J. Environ. Sci.*, 2012, **24(3)**, 449-457.

15 S. Kohtani, J. Hiro, N. Yamamoto, A. Kudo, K. Tokumura and R. Nakagaki, *Catal.Commun.*, 2005, **6**, 185-189.

16 H. Q. Jiang, H. Endo, H. Natori, M. Nagai and K. Kobayashi, *J. Eur. Ceram. Soc.*, 2008, **28**, 2955-2962.

17 A. Kudo, K. Ueda, H. Kato and I. Mikami, *Catal. Lett.*, 1998, **53**, 229-230.

18 M. Long, W. M. Cai, H. Kisch, *J. Phys. Chem. C*, 2008, **112**, 548-554.

19 K. Sayama, A. Nomura, Z.G. Zou, R. Abe, Y. Abe and H. Arakawa, *Chem.Commun.*, 2003, **23**, 2908-2909.

20 Y.Yang, Q.Zhang, B.Zhang, W.B.Mi, L.Chen, L.Li, C.Zhao, E.M.Diallo, X.X.Zhang, *Appl. Surf. Sci*. 2012, **258**, 4532-4537.

21 L. S. Kumari and P.P. Rao, A. N. P. Radhakrishnan, V. James, S. Sameera, P. Koshy, *Sol. Energy Mater.Sol. Cells*, 2013, **112**, 134-143.

22 F. D. Hardcastle and I.E. Wachs, *J. Phys. Chem*, 1991, **95**, 5031-5041.

23 (a) W. Ma, Z. Lu and M. Zhang, *Appl. Phys. A*, 1998, **66**, 621-627; (b) J. Yu, A. Kudo, Adv. Funct. Mater. 2006, **16**, 2163–2169.

24 (a) J.Yu and A.Kudo, *Adv. Funct. Mater*.,2006, **16(16)**, 2163-2169; (b) A.P.Zhang, J.Z.Zhang, N.Y.Cui, X.Y.Tie, Y.W. An and L.J.Li, *J. Mol. Catal. Chem.*, 2009, **304**, 28-32.

25 M. Wang, Q. Liu, Y. Che and D. Zhang, *J. Alloy compd.*, 2013, **548**, 70-76.

26 H.Y. Jiang, H. X. Dai, X. Meng, L. Zhang, J.G. Deng and K. M. Ji, *Chinese. J. Catal.*, 2011,**32(6)**, 939-949.

27 (a) A. Kudo, R. Niishiro, A. Iwase and H. Kato, *Chem. Phys.*, 2007, **339(1-3)**, 104-110; (b) A. Walsh, Y. Yan, M. N. Huda, M. M. Al-Jassim and S. H. Wei, *Chem.Mater*., 2009, **21**, 547-551.

28 K. Ordon, V. Merupo S. Velumani, A. Kassiba, M. Makowska-Janusik, *Inorg.Chem, submitted*, 2015, ic-2015-00079v

29 A. P. Zhang and J. Z. Zhang, *Acta Phys. Chim. Sin.*, 2010, **26**, 1337-1342.

CrystEngComm Accepted Manuscript

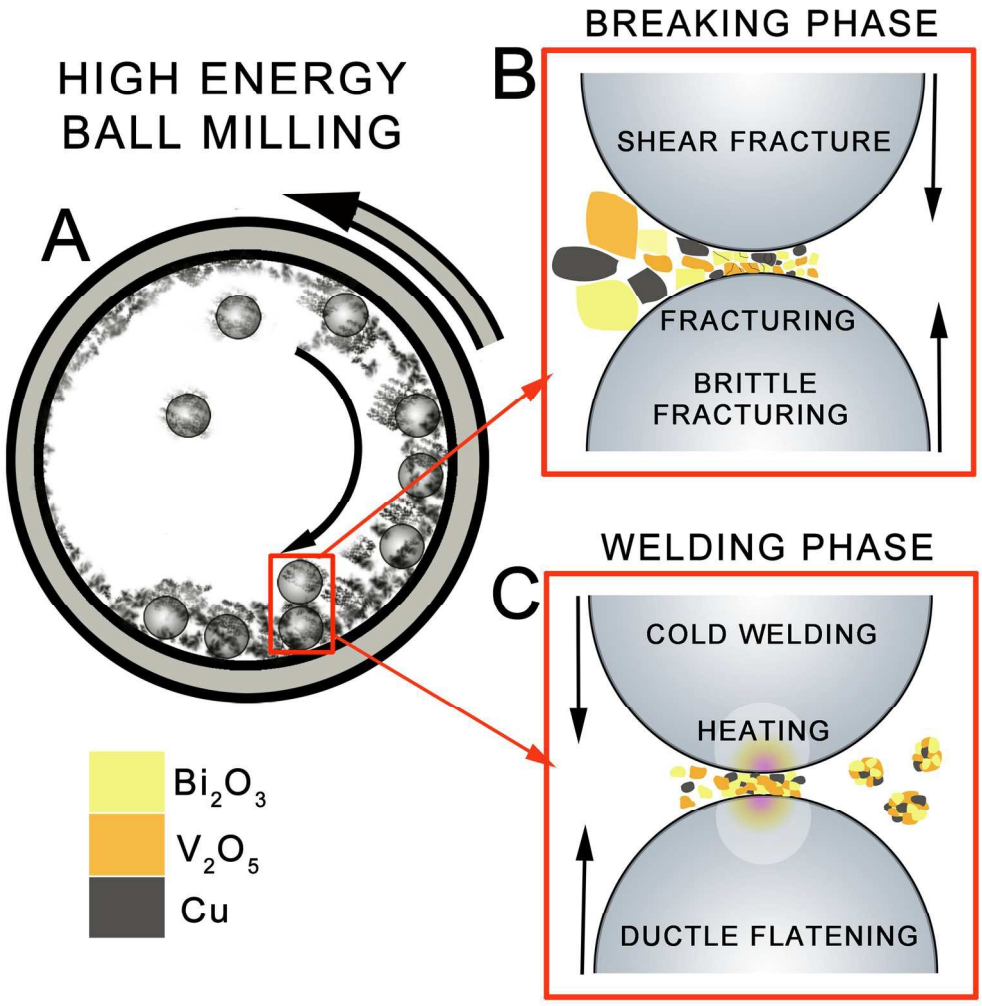

Fig.1 Schematic representation of high energy ball milling synthesis mechanism for Cu doped BiVO4 nanoparticle: (A) shows the content of the rotating (rpm) reaction chamber with hard balls and mixture of the initial reactants at defined stoichiometric ratios which define the final product. (B) illustrates the breaking phase, where repeated fracturing of bulk reactants cause formation of composite particles with desired composition. (C) shows the welding phase, where small agglomeration of particles form the final morphology of the powder.
85x87mm (600 x 600 DPI)

CrystEngComm Accepted Manuscript

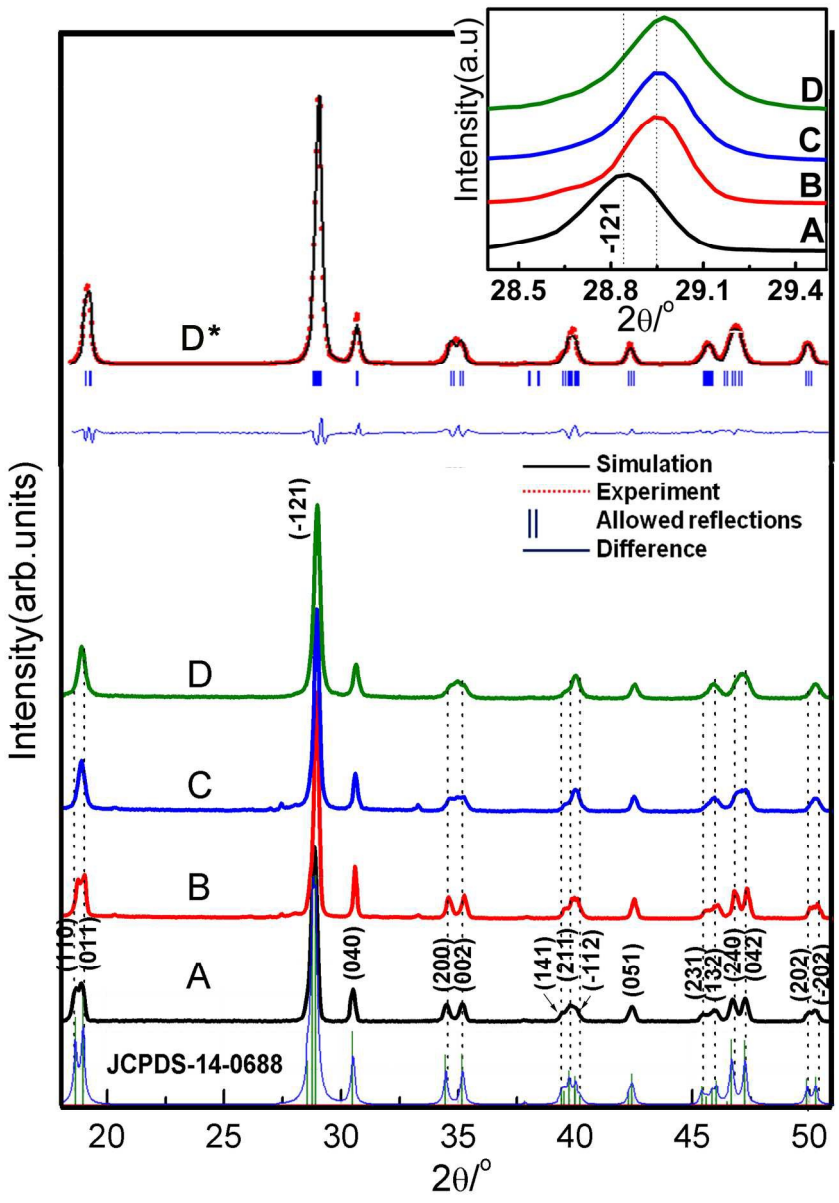

Fig.2 X-ray diffraction patterns of copper doped BiVO4 nanopowders with different Cu doping ratios. The bottom pattern represents the reference diffraction pattern for monoclinic scheelite BiVO4 referred as JCPDS-14-0688. Samples labelled as A, B, C and D correspond to undoped BiVO4, 1 at.%, 5 at.% and 10 at.% of Cu-BiVO4 respectively. D* represents FullProf refinement for 10 at% Cu-BiVO4. The inset shows the shift of 2θ towards higher angle for characteristic peak corresponding to (-121) plane
114x157mm (600 x 600 DPI)

CrystEngComm Accepted Manuscript

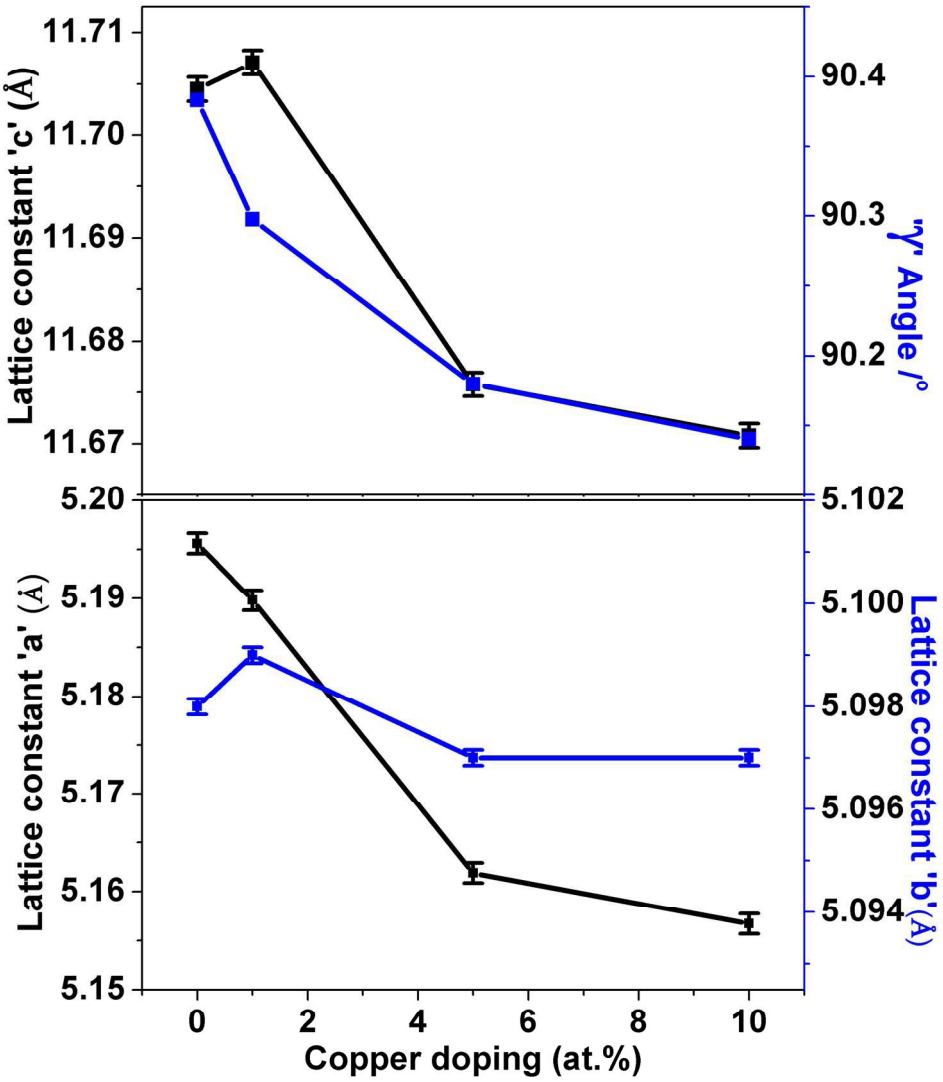

Fig.3 Crystallographic lattice parameters obtained from refined XRD patterns by Rietveld method for Cu-BiVO4 samples.
95x109mm (600 x 600 DPI)

CrystEngComm Accepted Manuscript

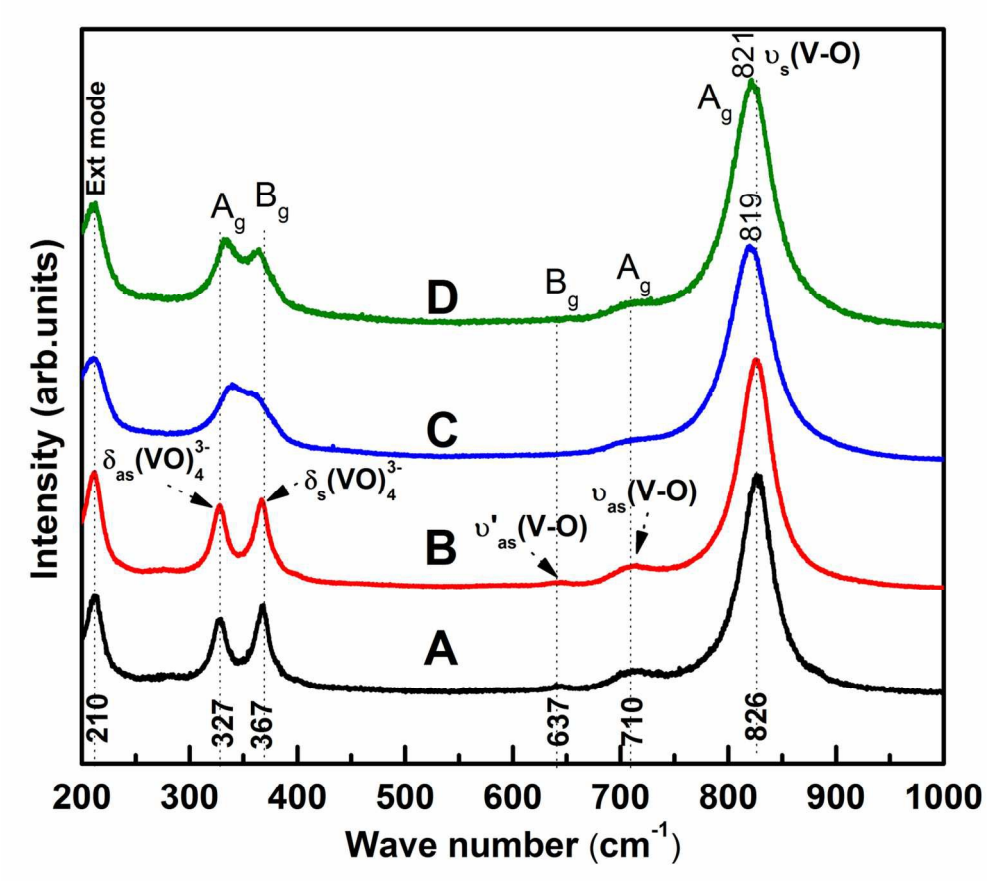

Fig.4 Raman spectra of copper doped BiVO4 samples with the assignment of stretching and bending modes with their respective notations. Samples are referred as A, B, C and D for undoped BiVO4, 1 at.%, 5 at.% and 10 at.% of Cu-BiVO4 respectively.
63x56mm (600 x 600 DPI)

CrystEngComm Accepted Manuscript

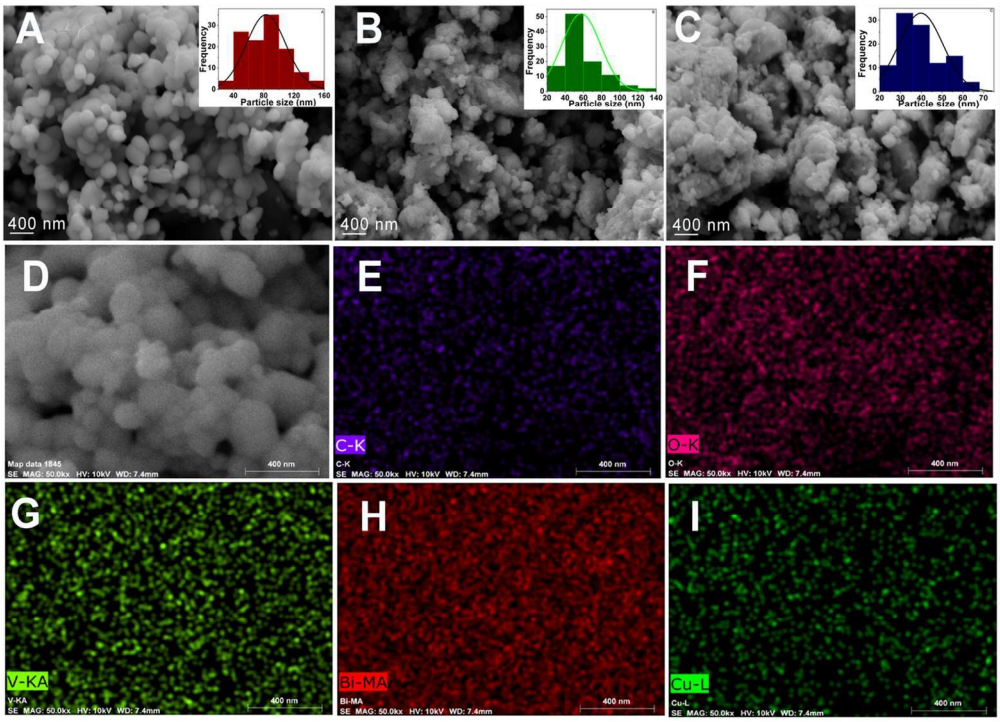

Fig.5. FE-SEM images of copper doped BiVO4 nanopowders for (A): 1 at.%, (B:) 5 at.%, (C): 10 at.%. inset with particle size distribution. Elemental mapping from EDAX composition profile for 5 at.% in Cu-BiVO4 sample (D). (E): Carbon K-line from substrate, (F): Oxygen K-line, (G): Vanadium K-alpha line, (H): Bismuth M-alpha line and (I): Copper L-line
60x43mm (600 x 600 DPI)

CrystEngComm Accepted Manuscript

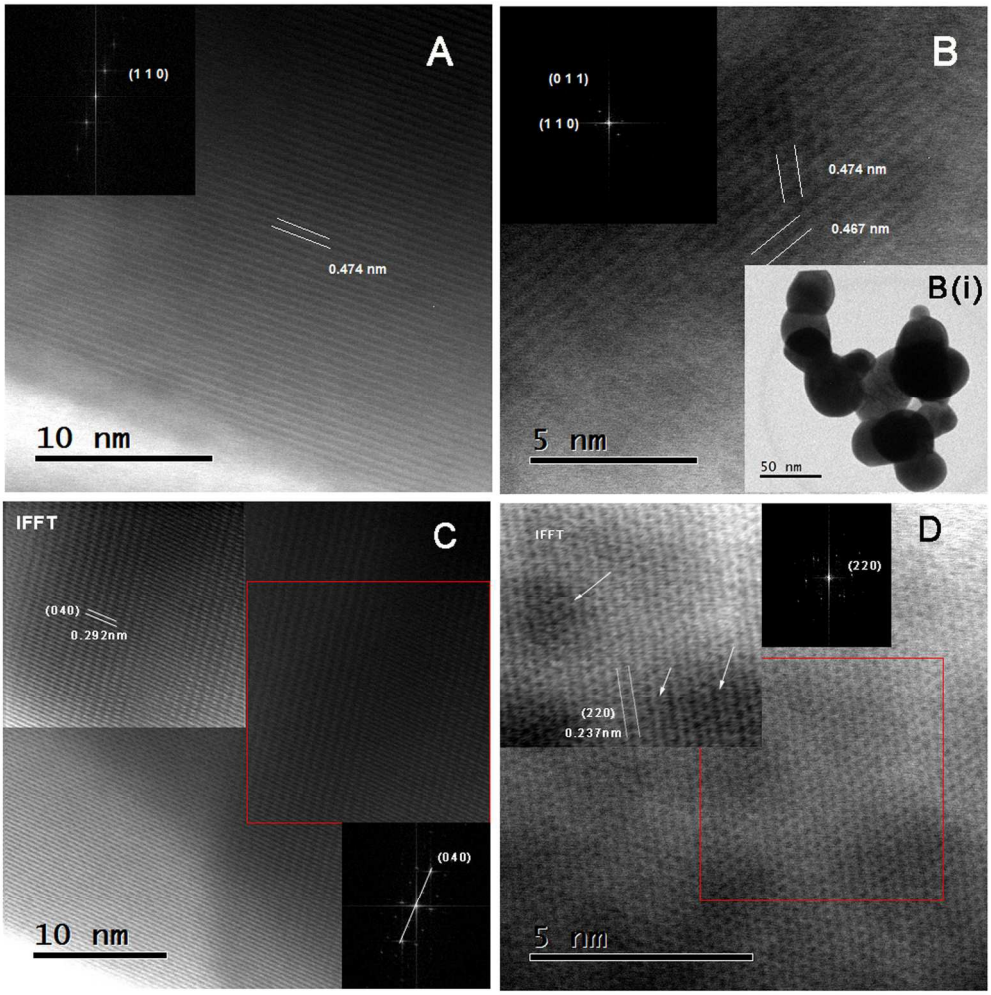

Fig.6 HR-TEM images with corresponding FFT in inset for copper doped Cu-BiVO4 samples. (A): undoped, (B): 1 at.% with inset (i) of particle size around 50nm, (C): 5 at.% with inset of IFFT image and (D): 10 at.% with inset of IFFT image showing distorted lattice indicated by arrows
83x83mm (600 x 600 DPI)

CrystEngComm Accepted Manuscript

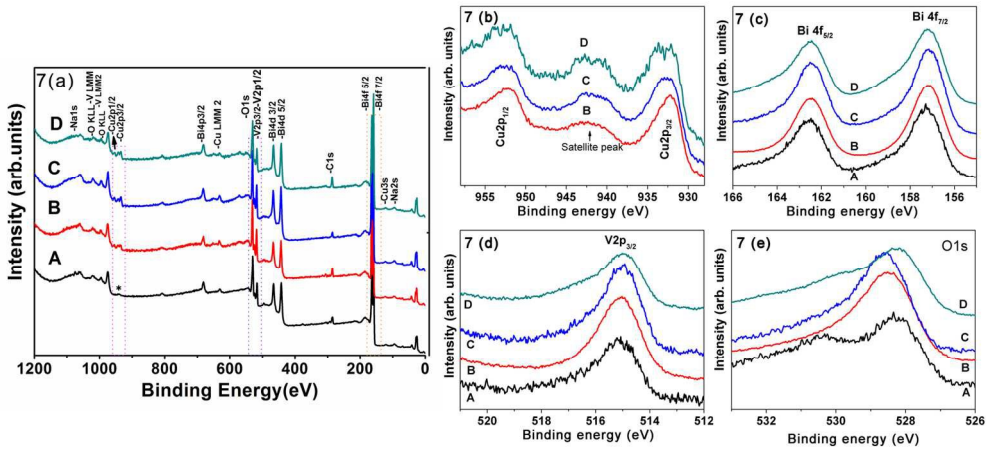

Fig.7 XPS spectra for undoped and Cu doped BiVO4 samples where A, B, C and D are associated to undoped BiVO4, 1 at.%, 5 at.% and 10 at.% Cu-BiVO4 respectively; (b, c, d & e) illustrate the binding energies of Cu 2p, Bi 4f, O 1s and V 2p orbitals.
77x34mm (600 x 600 DPI)

CrystEngComm Accepted Manuscript

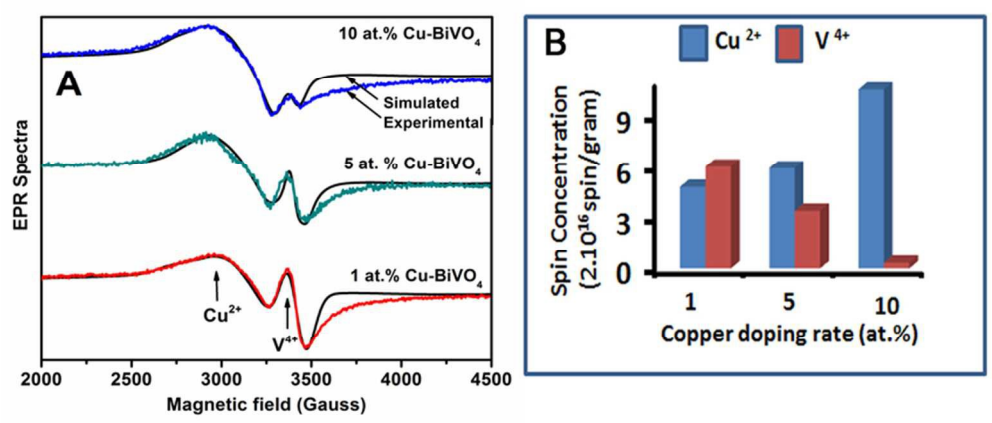

Fig.8(A) EPR spectra of copper doped BiVO4 samples with different copper doping rates. (B) Absolute concentrations of Cu2+ and V4+ ions and their evolution with copper doping rate.
36x15mm (600 x 600 DPI)

CrystEngComm Accepted Manuscript

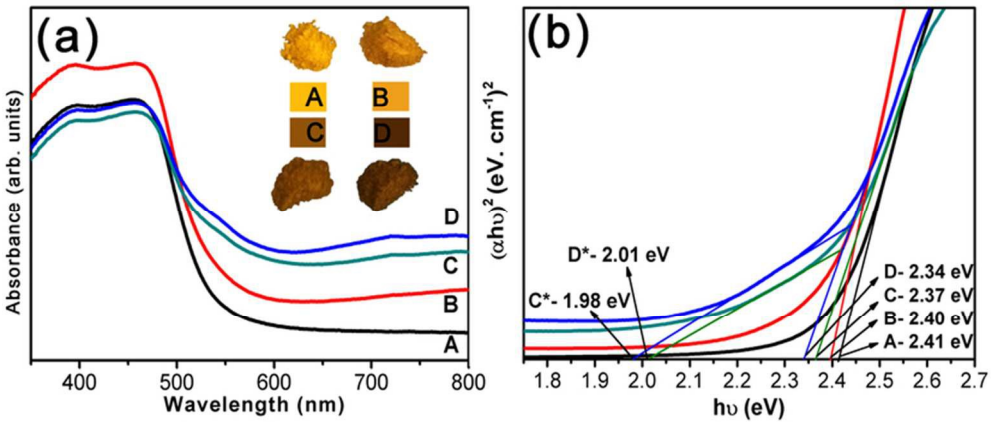

Fig.9(a) UV-Vis diffuse absorption spectra of BiVO4 samples; (A): undoped BiVO4 (B): 1 at.%, (C): 5 at.% and D: 10 at.% in Cu-BiVO4 respectively. The inset (A) shows the color of Cu doped BiVO4 powders with different Cu concentrations and (b) reports the band gap energy values for Cu doped BiVO4 obtained from Tauc plot.
35x14mm (600 x 600 DPI)

CrystEngComm Accepted Manuscript

Table1 Calculated coherent diffracting domains from Scherrer's formula and optical band gap values of Cu-$BiVO_4$ samples.

samples	FWHM	2θ position (-121)	Crystallite size(nm)	Band gap E_g(eV)
$BiVO_4$	0.220	28.86	37.78	2.41
1at.% Cu-$BiVO_4$	0.206	28.946	40.49	2.40
5at.% Cu-$BiVO_4$	0.231	28.958	35.9	2.37
10at.% Cu-$BiVO_4$	0.2505	28.973	33.03	2.34

CrystEngComm Accepted Manuscript

Table 2a Phase composition and crystallographic lattice parameters of monoclinic Cu doped $BiVO_4$nanopowders, refined by Rietveld method from X- ray powder diffraction patterns.

	Phase fraction				Crystal lattice parameters			
Sample name	$BiVO_4$	Bi_2O_3	V_2O_5	Crystal size(nm)	a(Å)	b(Å)	c(Å)	γ(°)
1at%Cu-$BiVO_4$	98.6 (±0.02)	1.3 (±0.008)	0 (±0)	43	5.189 ($\pm3.2e^{-4}$)	5.100 ($3.2e^{-4}$)	11.707 ($6.4e^{-4}$)	90.297
5at%Cu-$BiVO_4$	97.6 (±0.02)	2.3 (±0.004)	0 (±0)	40	5.161 ($\pm4.2e^{-4}$)	5.097 ($4.1e^{-4}$)	11.675 ($8.4e^{-4}$)	90.1806
10at%Cu-$BiVO_4$	100 (±0.03)	0 (±0)	0 (±0)	31	5.156 ($\pm4.5e^{-4}$)	5.097 ($4.3e^{-4}$)	11.607 ($9.1e^{-4}$)	90.1406

CrystEngComm Accepted Manuscript

Table 2b Atomic positions of monoclinic phase in Cu doped $BiVO_4$ nanopowders refined by Rietveld method.

Sample name	Bi			V			O1			O2		
1at.%Cu-$BiVO_4$	0	0.249	0.632	0	0.25	0.128	0.144	0.472	0.2019	0.325	0.353	0.429
	(±0.002-0.003)			(±0.002-0.003)			(±0.002-0.003)			(±0.002-0.003)		
5at.%Cu-$BiVO_4$	4.7e-4	0.25	0.63	0.01	0.315	0.111	0.137	0.55	0.22	0.278	0.384	0.428
	(±0.002-0.003)			(±0.002-0.003)			(±0.002-0.003)			(±0.002-0.003)		
10at.%Cu-$BiVO_4$	2.5e-4	0.249	0.635	0.012	0.31	0.116	0.132	0.55	0.216	0.28	0.383	0.435
	(±0.002-0.003)			(±0.002-0.003)			(±0.002-0.003)			(±0.002-0.003)		

CrystEngComm Accepted Manuscript

Table3 Energy dispersive X-ray spectroscopy showing chemical compositions for Cu-$BiVO_4$ samples.

Cu (at. %) Experimental	Bismuth (at. %)	Vanadium (at. %)	Oxygen (at. %)	Cu (at. %) (EDAX)
0	16.46	17.54	66.0	-
1	15.36	15.66	67.99	0.99
5	18.88	19.36	59.94	1.82
10	19.09	18.87	59.28	2.76

CrystEngComm Accepted Manuscript

Graphical abstract

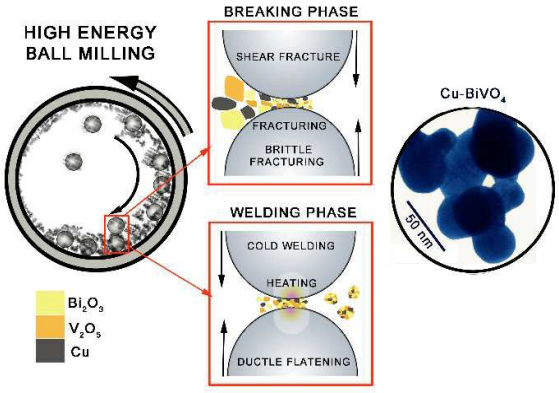

Novelty of work:

Mechano-chemical synthesis of Cu doped $BiVO_4$ monoclinic nanopowders and investigation of structural, optical and electronic properties.

CrystEngComm Accepted Manuscript